⌘ *Author's Choice*

THE JOURNAL OF BIOLOGICAL CHEMISTRY VOL. 285, NO. 50, pp. 39458–39470, December 10, 2010

A Molecular Switch between the Outer and the Inner Vestibules of the Voltage-gated Na^+ Channel*[S]

Received for publication, April 11, 2010, and in revised form, September 3, 2010 Published, JBC Papers in Press, October 6, 2010, DOI 10.1074/jbc.M110.132886

Touran Zarrabi[‡], Rene Cervenka[‡], Walter Sandtner[‡], Peter Lukacs[‡], Xaver Koenig[‡], Karlheinz Hilber[‡], Markus Mille[‡], Gregory M. Lipkind[§], Harry A. Fozzard[§], and Hannes Todt[‡1]

From the [‡]Center for Physiology and Pharmacology, Institute of Pharmacology, Medical University of Vienna, Vienna 1090, Austria and [§]Cardiac Electrophysiology Laboratories, Department of Medicine, The University of Chicago, Chicago, Illinois 60637

Voltage-gated ion channels are transmembrane proteins that undergo complex conformational changes during their gating transitions. Both functional and structural data from K^+ channels suggest that extracellular and intracellular parts of the pore communicate with each other via a trajectory of interacting amino acids. No crystal structures are available for voltage-gated Na^+ channels, but functional data suggest a similar intramolecular communication involving the inner and outer vestibules. However, the mechanism of such communication is unknown. Here, we report that amino acid Ile-1575 in the middle of transmembrane segment 6 of domain IV (DIV-S6) in the adult rat skeletal muscle isoform of the voltage-gated sodium channel ($rNa_V1.4$) may act as molecular switch allowing for interaction between outer and inner vestibules. Cysteine scanning mutagenesis of the internal part of DIV-S6 revealed that only mutations at site 1575 rescued the channel from a unique kinetic state ("ultra-slow inactivation," I_{US}) produced by the mutation K1237E in the selectivity filter. A similar effect was seen with I1575A. Previously, we reported that conformational changes of both the internal and the external vestibule are involved in the generation of I_{US}. The fact that mutations at site 1575 modulate I_{US} produced by K1237E strongly suggests an interaction between these sites. Our data confirm a previously published molecular model in which Ile-1575 of DIV-S6 is in close proximity to Lys-1237 of the selectivity filter. Furthermore, these functional data define the position of the selectivity filter relative to the adjacent DIV-S6 segment within the ionic permeation pathway.

Ion channels are transmembrane proteins that regulate the flow of ions across the cell membrane. This process is central to the modulation of cell excitability and to the transduction of signals across the membrane. Currently crystal structures of the voltage-gated Na^+ channel are not available; however, the general topology of these proteins is believed to be homologous to published crystal structures of K^+ channels. The common motif of these ion channels includes four subunits or domains arranged symmetrically around the central ion-conducting pore. Each subunit or domain contains at least two transmembrane α-helices separated by a membrane re-entrant loop (P-loop) incorporating the selectivity filter (outer vestibule). The four inner α-helices corresponding to the S6 segments in voltage-gated Na^+ channels form the central pore (inner vestibule) and contain the activation gate. The segment of the P-loop immediately N-terminal to the selectivity filter forms an α-helix ("pore helix") that is in close proximity to the inner pore-lining α-helix (1, 2).

The transmembrane activity of ion channels requires some form of intramolecular communication between the extracellular (*i.e.* the outer vestibule) and intracellular parts. A number of functional studies in voltage-gated K^+ channels suggest an interaction between the pore-lining α-helices of the internal vestibule and the P-loop region of the external vestibule (3–7). Recently, Cuello *et al.* (8, 9) solved the structure of the bacterial KcsA channel in different open conformations corresponding to varying states in the activation-inactivation pathway. Analysis of these structures suggested that residue Phe-103 in the inner pore-lining helix interacts with the C-terminal end of the pore helix resulting in a structural change that leads to a non-conductive conformation of the selectivity filter (8, 9). These structural data for the first time confirmed that in K^+ channels some forms of inactivation encompass an interaction between the outer vestibule (P-loops) and the inner helices (corresponding to the S6 segment of voltage-gated Na^+ channels).

Although evolutionally related to K^+ channels, the predicted structure of Na^+ channels differs in important aspects from the K^+ channel structure. For example, the tetrameric arrangement of separate subunits in K^+ channels is replaced by a four-domain composition of a single chain in Na^+ channels. Furthermore, amino acids of the P-loops are proposed to direct their side chains towards the permeation pathway in Na^+ channels, whereas these side chains point away from the pore in the K^+ channel crystal structures (2). It is likely that these structural variations between K^+ channels and Na^+ channels affect their mode of intraprotein transmembrane communication.

A published homology model of the voltage-gated Na^+ channel, based on the crystal backbone structure of the KcsA K^+ channel, suggests a close spatial relationship between the base of the P-loops forming the selectivity filter and the S6 segments lining the internal vestibule (2). We wondered

* This work was supported, in whole or in part, by National Institutes of Health Grant 1R01 HL096476-01. This work was also supported by Austrian Science Fund Grants P21006-B11, P17509-B11, and P13961-B05.

⌘ *Author's Choice*—Final version full access.

[S] The on-line version of this article (available at http://www.jbc.org) contains supplemental Table 1.

[1] To whom correspondence should be addressed: Institute of Pharmacology, Medical University of Vienna, Waehringerstrasse 13a, 1090 Vienna, Austria. Tel.: 43-1-4277-64120; Fax: 43-1-4277-9641; E-mail: hannes.todt@meduniwien.ac.at.

whether, as in K^+ channels, the selectivity filter and the inner helices (S6 segments) are part of an intramolecular signal transduction pathway allowing for transmembrane communication. For this purpose we exploited a very specific protein conformation of the $rNa_V1.4$ Na^+ channel that we refer to as ultra-slow inactivation (I_{US} (10)).[2] Previously, we reported that the likelihood of entry into I_{US} is substantially increased by the mutation in the selectivity filter, K1237E (10–12). I_{US} can be modulated by molecules binding to the outer vestibule (10, 12), suggesting that a conformational change of the outer vestibule gives rise to this kinetic state. On the other hand, the I_{US} state can be modulated by binding of the inactivation lid to the internal vestibule (11). Furthermore, the local anesthetic drug lidocaine, which binds to the internal part of the channel pore (13), inhibits entry into I_{US} by a "foot-in-the-door" mechanism (14), indicating that a closure of the inner vestibule is involved in the generation of I_{US}. To explain the involvement of both the outer and the inner vestibule in I_{US}, we proposed a model in which the mutation K1237E produces a conformational change of the outer vestibule, which is transmitted to the internal vestibule through the DIV-S6 segment (12, 14, 15). Hence, the mechanism of inactivation may be analogous to the one proposed by Cuello *et al.* (8, 9) for the KcsA channel, in which residue Phe-103 in TM2 interacts with the selectivity filter. In voltage-gated Na^+ channels the S6 segment corresponds to TM2 in KcsA. Here, we present the results of a cysteine-scanning mutagenesis of the intracellular part of the S6 segment of domain IV (DIV-S6) to detect a possible interaction site with the selectivity filter. We find that I_{US} generated by a mutation in the selectivity filter of the $rNa_V1.4$ channel (K1237E) can be abolished by an additional mutation at the site 1575 in DIV-S6. This effect is unique to site 1575 because no other mutation in the DIV-S6 was able to remove the I_{US} state. In a previously published homology model Ile-1575 of DIV-S6 is in close spatial proximity to the side chain of Lys-1237 of the DIII P-loop, suggesting an interaction between these amino acids (2). These data support the idea of a trans-protein communication via the selectivity filter and the adjacent inner helices. Furthermore, in the absence of a crystal structure for the voltage-gated Na^+ channel, our functional data for the first time determine the position of the selectivity filter in the pore relative to the DIV-S6 segment.

EXPERIMENTAL PROCEDURES

Mutagenesis of $rNa_V1.4$—A vector consisting of the $rNa_V1.4$ coding sequence flanked by *Xenopus* globin 5′- and 3′-untranslated regions was provided as a gift by R. Moorman (University of Virginia, Charlottesville, VA). This was used as the template for inserting oligonucleotide-directed point mutations by either four primer PCR and subsequent subcloning into the template using directional ligations or the QuikChange site-directed mutagenesis kit (Stratagene, La Jolla, CA). Oligonucleotide primers containing a mutation were designed with a change in a silent restriction site to allow rapid identification of the mutant. Incorporation of the mutation into the template was then confirmed by DNA sequencing. Double mutants were made by subcloning the region of the DIV-S6 segment that contained the mutation into the $rNa_V1.4$-K1237E construct. All constructs were linearized by either SpeI or SalI and transcribed with either T7 (SpeI-linearized) or SP6 (SalI-linearized) RNA polymerase using the respective mMessage mMachine Kits according to the manufacturer's protocols (Ambion, Austin, TX).

Oocyte Preparation—Stage V and VI *Xenopus* oocytes were isolated from female frogs (NASCO, Ft. Atkinson, WI), washed with a solution containing 96 mM NaCl, 2 mM KCl, 20 mM $MgCl_2$, and 5 mM HEPES (titrated to pH 7.4 with 10 M NaOH), treated with 1 mg/ml collagenase for 0.5 to 1 h, and had their follicular cell layers manually removed. As judged from photometric measurements, ~50–100 ng of cRNA were injected into each oocyte with a Drummond micro-injector (Broomall, PA). Oocytes were incubated at 17.5 °C for 8 h to 14 days before examination in a solution containing 90 mM NaCl, 2 mM KCl, 1 mM $MgCl_2$, 5 mM Hepes, 1.8 mM $CaCl_2$, 2.5 mM sodium pyruvate, and 1 g/liter dextrose. All chemicals were of the purest grade available and were purchased from Sigma.

Electrophysiological Recordings—Recordings were made in the two-electrode voltage clamp configuration using a TEC 10CD clamp (npi electronic, Tamm, Germany). The clamp amplifier had a series resistance compensation circuit. For accurate adjustment of the experimental temperature (18 ± 0.5 °C), an oocyte bath cooling system (HE 204, Dagan, Minneapolis, MN) was used. Oocytes were placed in recording chambers in which the bath flow rate was about 100 ml/h, and the bath level was adjusted so that the total bath volume was less than 500 μl. Electrodes were filled with 3 M KCl and had resistances of less than 0.5 megaohms. Using pCLAMP6 (Axon Instruments, Foster City, CA) software, data were acquired at 71.4 kHz after low-pass filtration at 2 kHz (−3 decibel). Curve-fitting was performed using OriginPro 7.5 (MicroCal Software Inc., Northampton, MA). Recordings were made in a bathing solution that consisted of 90 mM NaCl, 2.5 mM KCl, 1 mM $BaCl_2$, 1 mM $MgCl_2$, and 5 mM HEPES titrated to pH 7.4 with 10 M NaOH. $BaCl_2$ was used as a replacement for $CaCl_2$ to minimize Ca^{2+}-activated Cl^- currents.

For the experiments in which Na^+ was replaced by other monovalent cations, 90 mM NaCl in the standard extracellular solution was replaced by 90 mM of the respective test cation as chloride salt, and the buffer was titrated with Tris base. The following chemicals were used for these experiments: choline chloride, methylamine hydrochloride, and diethylamine hydrochloride (all from Sigma).

Molecular Modeling—Modeling was accomplished in the Insight and Discover graphical environments (Biosym Technologies Inc., San Diego, CA) as described previously (16). The homology-modeled structure of the pore of the Na^+ channel was fixed in all calculations except for the side chains of the amino acid residues forming the selectivity filter, Asp-400, Glu-755, Lys-1237 and Ala-1529.

Data Evaluation—If not otherwise specified, recovery from I_{US} was tested with the following experimental protocol, as

[2] The abbreviations used are: I_{US}, ultra-slow inactivation; DI-DIV, domains I-IV; $rNa_V1.4$, adult rat skeletal muscle isoform of the voltage-gated sodium channel.

reported previously (10). From a holding potential of −120 mV, the channels were inactivated by a 300-s depolarizing voltage step to −20 mV. This prepulse duration, rather than longer ones, was normally chosen to avoid unacceptably long experimental durations. After the prepulse, the potential was returned to −120 mV, and recovery from inactivation was monitored by repetitive 20-ms test pulses to −20 mV at 20-s intervals. The first test pulse was applied 20 s after the prepulse to allow for recovery from faster forms of inactivation (fast and slow inactivation). The time courses of recovery from I_{US} of normalized peak inward currents were fit with the bi-exponential function (Equation 1),

$$I_2/I_1 = -A_1 \exp(-t/\tau_1) - A_2 \exp(-t/\tau_2) + C \quad \text{(Eq. 1)}$$

where I_2 is the peak inward Na^+ current of the test pulse during recovery, I_1 is the peak inward Na^+ current of a test pulse under fully available conditions, τ_1 and τ_2 are the time constants of distinct components of recovery from inactivation (slow inactivation and I_{US}, respectively), A_1 and A_2 are the respective amplitudes of these time constants, and C is the final level of recovery. A_2 was taken as a measure of the fraction of channels that recovered from I_{US}.

Current-voltage relationships were fit with the function (Equation 2),

$$G_{max}(V - V_{rev})(1 - (1/(1 + \exp((V - V_{0.5})/K)))) \quad \text{(Eq. 2)}$$

where V is the step potential, G_{max} is the maximum conductance, $V_{0.5}$ is the voltage at which half-maximum activation occurred, V_{rev} is the reversal potential, and K is the slope factor.

The permeability ratio of choline was computed relative to 90 mM Na^+ from the change in the reversal potential observed in going from the bath solution containing 90 mM Na^+ to the bath solution in which 90 mM Na^+ was replaced by 90 mM choline, according to Tsushima *et al.* (17; Equation 3).

$$P_{choline}/P_{Na^+} = [Na^+]/[choline]\exp(\Delta V/\alpha) \quad \text{(Eq. 3)}$$

where $\Delta V = V_{choline} - V_{Na^+}$, and $\alpha = RT/F = 25.4$ mV.

The picture in Fig. 12 was generated by the MVM graphics Program by ZMM Software Inc., Canada—Data are expressed as the means ± S.E.M. Statistical comparisons were made using two-tailed Student's *t* tests. A $p < 0.05$ was considered significant.

RESULTS

A Mutation in the Selectivity Filter Promotes Entry into I_{US}—Fig. 1 shows the time course of recovery from I_{US} produced by a 300-s depolarizing prepulse to −20 mV in wild type $rNa_V1.4$ channels and in the mutant K1237E. Currents through wild type channels recover completely within 40–60 s after the prepulse. As described previously (10), the mutation K1237E substantially prolongs the time course of recovery. The normalized time course can be fitted with two exponentials reflecting recovery from at least two inactivated states. The smaller time constant most likely corresponds to recovery from "slow inactivation" (18), whereas the greater time constant represents recovery from I_{US} (10). Charge-altering mutations of amino acids at homologous positions in other domains do not induce I_{US} by the applied protocol (Fig. 1*C*).

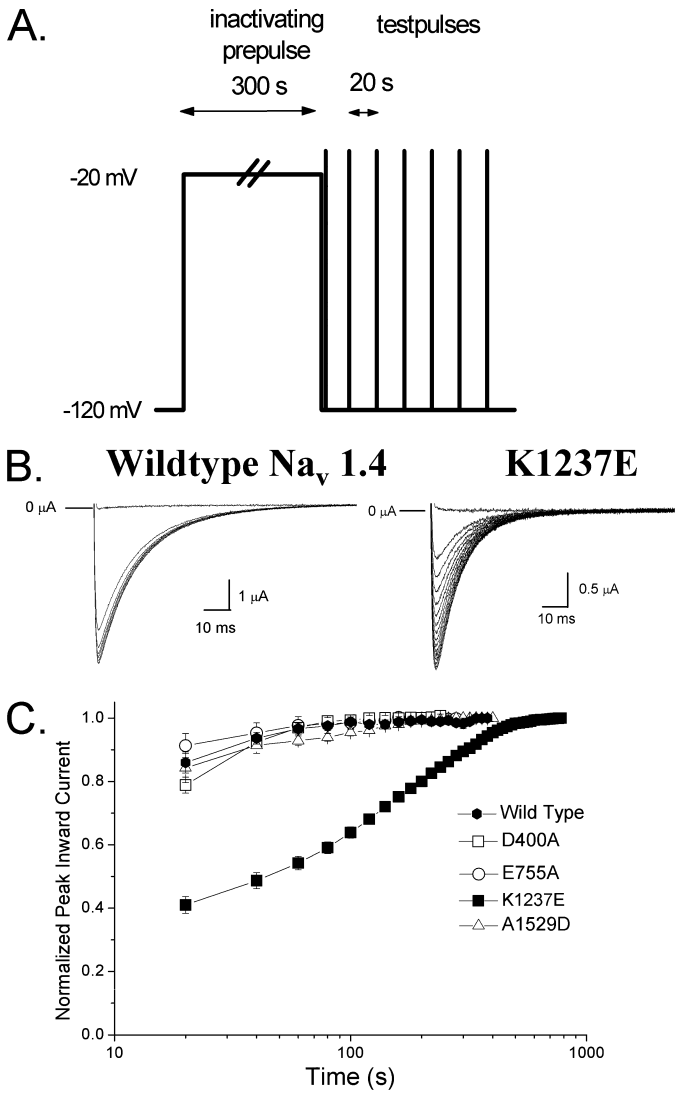

FIGURE 1. **The mutation K1237E produces an inactivated state from which recovery is very slow (I_{US}).** *A*, shown is a graphic representation of the voltage-clamp protocol for assessment of the time course of recovery from I_{US}. From a holding potential of −120 mV, the channels were inactivated by a 300-s depolarizing step to −20 mV. After return to −120 mV, recovery from inactivation was monitored by repetitive test pulses to −20 mV at 20-s intervals. *B*, shown are inward currents through wild type and K1237E channels elicited by test pulses after the holding potential was returned to −120 mV. Here, to allow for better resolution of the current traces, test-pulse duration was 100 ms. In both constructs the first test pulse failed to elicit inward current. With wild type channels the second test pulse resulted in almost full recovery, whereas in K1237E channels full recovery was not attained before ~300 s had elapsed. *C*, shown is the effect of charge-altering mutations of K1237E and of residues at homologous positions in DI, II, and IV. Oocytes expressing currents of the constructs D400A, E755A, and A1529D were subjected to the protocol shown in *A*. Currents are normalized to the value after full recovery and plotted as a function of time after the conditioning prepulse. Only the mutation K1237E results in substantial ultra-slow recovery.

Differential Kinetic Effects of Combining K1237E with Alanine Substitutions in DIV-S6—Molecular modeling predicts that Lys-1237 in the domain III P-loop is in close proximity to Ile-1575 of the DIV-S6 (Fig. 2*A*). If I_{US} occurred by an interaction between the P-loops and the adjacent S6 segment, then Ile-1575 is a likely partner for such an interaction. Therefore,

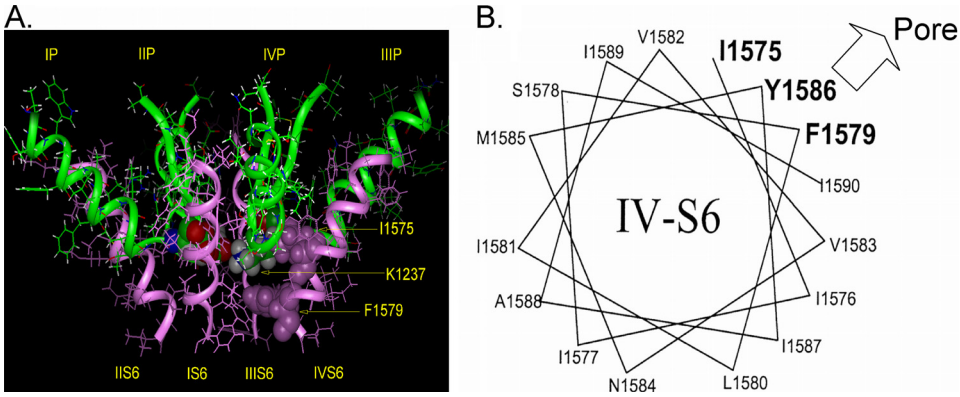

FIGURE 2. **Previously published molecular model of the voltage gated Na^+ channel (2).** The P loops are represented as *green ribbons*, S6 helices are presented as *pink ribbons*. *A*, amino acids Lys-1237 of the selectivity filter and Ile-1575 and Phe-1579 of DIV-S6 are shown by *space-filling models*. Amino acid numbering corresponds to the $rNa_V1.4$ channel. Amino acid Lys-1237 of the DIII P-loop is in close spatial relationship to amino acid Ile-1575 of the DIV-S6 segment. Phe-1579 is located one helix turn internal to Ile-1575 and lines the permeation pathway in the inner vestibule. *B*, shown is a helical wheel representation of the DIV-S6 segment. Only amino acids downstream of Ile-1575 are shown. Amino acids in *bold* are considered to face the permeation pathway.

we tested whether substitutions of the amino acid side chain at position 1575 affected the propensity of the mutant K1237E to enter into I_{US}. For control purposes we also explored the effect of mutating residues Phe-1579 and Tyr-1586, which are predicted to face the pore at more internal positions along the permeation pathway (2, 13).

Fig. 3*A* shows the normalized time course of recovery from a 300-s conditioning prepulse to −20 mV in K1237E and the previously mentioned double mutants. The data points were well fit with a bi-exponential function (Equation 1), and the parameters derived from the fits are shown in Table 1. I_{US} was substantially enhanced when K1237E was combined with F1579A and Y1586A. In fact, the amplitudes of I_{US} in these double mutants exceeded the amplitude of I_{US} in the single mutant K1237E. Most interestingly, however, when K1237E was combined with I1575A, the amplitude of I_{US} was not enhanced but was reduced to the wild type level (Table 1). Hence, whereas the addition of F1579A and Y1586A enhanced I_{US} in the background of K1237E, the combination with I1575A appeared to protect K1237E channels from entry into I_{US}.

Mutations in the DIV-S6 Segment Promote Entry into I_{US}—As mentioned above, the amplitude of I_{US} in the double mutants K1237E/F1579A and K1237E/Y1586A were larger than in the single mutant K1237E. This raises the question of whether mutations in DIV-S6 alone modulated I_{US}. Hence, we tested the single mutants I1575A, F1579A, and Y1586A for their effects on I_{US}. As shown in Fig. 3*B*, full recovery from inactivation produced by a 300-s conditioning pulse was achieved by the second to third test pulse, *i.e.* 40–60 s after the inactivating prepulse in WT and I1575A. In F1579A and Y1586A, however, full recovery did not occur after ~10 test pulses (200 s) had elapsed. As shown in Table 1, the amplitude of the slow recovering component, A_2, representing the fraction of channels recovering from I_{US}, was significantly greater with F1579A and Y1586A than with I1575A and wild type. Thus, the single mutants F1579A and Y1586A enhanced the propensity to enter the I_{US} state, although to a lesser degree than the mutant K1237E in the selectivity filter (Fig. 1). The fact that single mutations in the DIV-S6 segment enhance the propensity of $rNa_V1.4$ channels to enter I_{US} supports our hypothesis that both the inner and the outer vestibule of the channel are involved in the generation of this inactivated state (14).

Most Cysteine Replacements in DIV-S6 Promote Entry into I_{US}—One explanation for the differential effect of the mentioned S6 substitutions on I_{US} is suggested by the molecular model shown in Fig. 2*A*. In this model Ile-1575 in DIV-S6 is in close proximity to Lys-1237 in the selectivity filter. The mutation K1237E has been shown to increase the permeability for large cations, suggesting that this mutation increases the diameter of the selectivity filter (19, 20). Most likely, this increase in diameter is produced by a "lateral swinging" of Glu-1237 (Ref. 21; Fig. 4). Such a conformational change is reasonable because the P-loops have been shown to be flexible structures in studies involving paired cysteine substitutions that allow disulfide bond formation (22, 23). The lateral motion of Glu-1237 may then alter the nature of the interaction with the neighboring S6 residue Ile-1575 (Fig. 4*B*). In the double mutant K1237E/I1575A changes in the properties of the side chain of Ala-1575 may alter the nature of interaction with Glu-1237, thereby protecting this mutant from entry into I_{US}. To further test this idea we introduced a cysteine at site 1575. The side chain of cysteine is both larger and more reactive than that of alanine. Presumably, replacement of the native amino acids by cysteine will impose greater structural changes in DIV-S6 than mutations to alanine. Furthermore, we wanted to test whether amino acid replacements at sites in the DIV-S6 segment more internal to 1575 were also capable of protecting K1237E from entry into I_{US}. To this end we produced serial cysteine replacements of all residues C-terminal to Ile-1575 in the DIV-S6 segment in the background of the wild type $rNa_V1.4$ channel and in the background of the mutation K1237E. Fig. 5 shows the amplitude of I_{US} produced by a 300-s depolarization to −20 mV in single cysteine replacements of amino acids in DIV-S6. I1576C and N1584C did not express sufficient current in order to be studied. Most of the remaining mutants had moderately higher amplitudes of I_{US} than wild type but significantly less than K1237E. As with I1575A, I1575C had a similar amplitude of I_{US} as wild type.

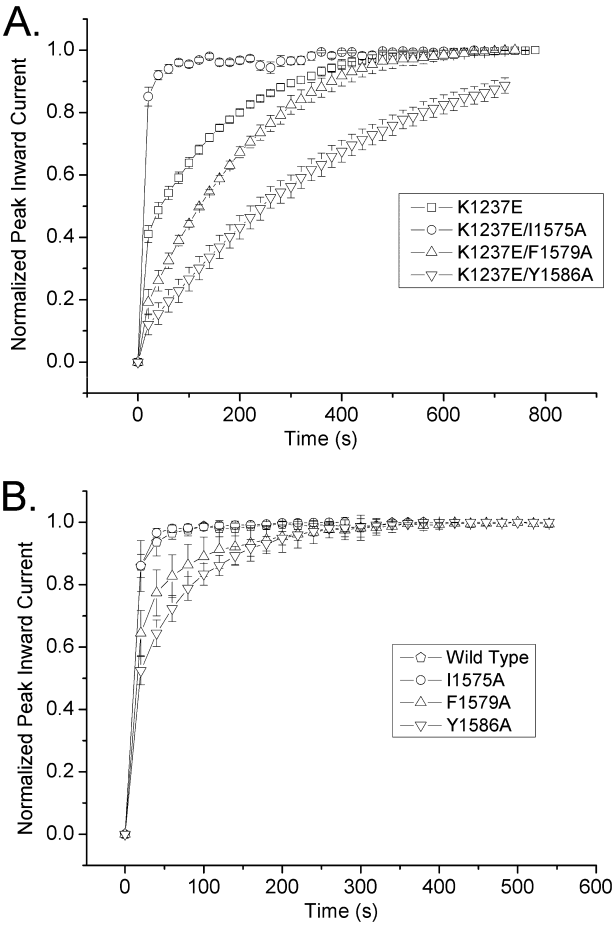

FIGURE 3. **I_{US} is modulated by mutations in the DIV-S6 segment.** Time course of recovery from a 300-s conditioning prepulse to −20 mV. Experimental protocol was as in Fig. 1. Maximum inward currents during recovery were normalized to the level after full recovery ($n = 6–8$). Data points were fitted with Equation 1 (*lines*). Fitting parameters are presented in Table 1. *A*, shown is a comparison of the time course of recovery of K1237E channels and the combination of K1237E with the DIV-S6 mutants I1575A, F1579A, and Y1586A. These amino acids in DIV-S6 are considered to face the pore (Fig. 2*B*) and are, thus, likely candidates for interaction with site 1237 in the DIII P-loop. Whereas the addition of F1579A and Y1586A enhanced recovery from I_{US} in K1237E background, the addition of I1575A protected K1237E channels from entry into the I_{US} state. *B*, shown is a comparison of the time course of recovery of wild type channels and the DIV-S6 mutants I1575A, F1579A, and Y1586A. F1579A and Y1586A show enhanced ultra-slow recovery, whereas the time course of recovery in I1575A is comparable with wild type channels.

Hence, among the mutated DIV-S6 sites, position 1575 appears to be unique in not enhancing the propensity of entry into I_{US}.

Kinetic Effects of Serial Cysteine Replacements in DIV-S6 in the Background of K1237E—The kinetic analysis of double mutants in which the K1237E background was combined with serial replacements of DIV-S6 amino acids C-terminal to Ile-1575 are presented in Figs. 6 and 7. As with the single mutants, all constructs except mutations at sites 1576 and 1584 expressed enough current to be studied. With one exception, all double mutants in DIV-S6 either did not affect I_{US} or produced an increase in the amplitude of I_{US}. Only in K1237E/I1575C did the fraction of channels recovering from I_{US} decrease significantly when compared with K1237E. However, whereas the replacement by alanine of Ile-1575 reduced the amplitude of I_{US} in K1237E to wild type levels (<20%, Table 1), introduction of a cysteine at site 1575 still allowed for entry of about 30% of channels into I_{US} (Fig. 7*B*), *i.e.* a percentage intermediate between wild type and K1237E. To further elucidate the kinetic changes imposed by the combination of K1237E with I1575C, we determined the effect of prolonging the duration of the inactivating prepulse on the fraction of channels recovering from I_{US}. This fraction was 0.34 ± 0.04 ($n = 6$), 0.33 ± 0.02 ($n = 4$), and 0.33 ± 0.02 ($n = 3$) after prepulse durations of 300, 600, and 900 s, respectively ($p =$ not significant). Thus, the fraction of channels recovering from I_{US} remained unchanged after increasing the duration of the conditioning prepulse, suggesting that I_{US} had attained steady state conditions after 300 s at −20 mV. Previously, we reported that I_{US} in K1237E is absorbing after ~ 600 s (10). Hence, the addition of I1575C to K1237E rendered I_{US} nonabsorbing, which indicates that I1575C severely destabilized the I_{US} state produced by K1237E. These data suggest that only mutations at site 1575 substantially reduce the stability of the I_{US} state.

Permeation by Organic Cations Increases the Fraction of Channels Recovering from I_{US} in K1237E—So far, the data support our notion that the replacement of the positively charged lysine at position 1237 in the selectivity filter gives rise to a conformational change in this region, resulting in an altered interaction between Glu-1237 and Ile-1575 of the adjacent DIV-S6 segment. As shown schematically in Fig. 4 the change in diameter of the selectivity filter by the mutation K1237E may be one critical factor in the generation of I_{US}. If this idea holds true, then the amplitude of I_{US} should be increased by a "further extension" of the diameter of the selectivity filter. Such increases in diameter of the selectivity filter may be achieved by "forcing" very large cations through the channel (21). This concept is similar to an induced fit associated with binding of a toxin to the outer pore of a channel (24). Mutations at site 1237 in the selectivity filter have previously been shown to allow for permeation of cations substantially larger than Na^+ (25). In Fig. 8 we show the effect of permeation of several cations larger than Na^+ on the amplitude of I_{US} in K1237E. Whereas the permeation by K^+ did not substantially alter the time course of recovery from I_{US}, all tested organic cations increased the amplitude and the time constant of recovery from I_{US} (Fig. 8). The increase in the amplitude of recovery from I_{US} showed a significant linear correlation with the diameter of the permeating cations, supporting the notion that an increase in the size of the selectivity filter gives rise to I_{US} (Fig. 8*B*).

Mutations at Site 1575, but Not at Position 1579, Alter the Selectivity of Permeation in K1237E—The fact that permeation by large cations increases the propensity of K1237E channels to enter the I_{US} state demonstrates that the size of the selectivity filter substantially influences the inactivation kinetics of the channel and supports a direct interaction between the selectivity filter and the DIV-S6 segment. However, we cannot exclude that a conformational change at the selectivity filter is allosterically transmitted to the I_{US} gate. On the other hand, a direct interaction of the selectivity filter and the I_{US} gate could likely result in a mutual interaction. Hence,

TABLE 1

Parameters derived from nonlinear curve fits of Equation 1 ("Experimental Procedures") to the time course of recovery from I_{US} as determined by the protocol shown in Fig. 1*A*

τ1, τ2, A1, A2 represent the time constants and amplitudes of recovery from slow inactivation and ultra-slow inactivation, respectively. Because of the small amplitude of recovery from I_{US} in wild type and K1237E/I1575, τ2 was fixed at 120 s during the curve-fitting procedure. Also, because of the small number of data points accounting for τ1, the presented values should be regarded as rough estimates.

	τ1	A1	τ2	A2
Wild type	7.05 ± 1.01	0.95 ± 0.01	120.00 ± 0.00	0.05 ± 0.01
K1237E	5.67 ± 0.81	0.36 ± 0.04[a]	183.92 ± 9.58[a]	0.64 ± 0.04[a]
I1575A	9.14 ± 0.60	0.96 ± 0.01	120.00 ± 0.00	0.04 ± 0.01
F1579A	11.71 ± 0.26	0.71 ± 0.04[a]	158.57 ± 26.02[a]	0.29 ± 0.04[a]
Y1586A	11.62 ± 0.76	0.51 ± 0.06[a]	127.88 ± 7.88[a]	0.49 ± 0.06[a]
K1237E/I1575A	6.90 ± 0.32	0.93 ± 0.02	120.00 ± 0.00	0.08 ± 0.02
K1237E/F1579A	9.24 ± 0.76	0.09 ± 0.04[a]	294.99 ± 65.36[a]	0.90 ± 0.04[a]
K1237E/Y1586A	8.00 ± 1.32	0.05 ± 0.01[a]	448.66 ± 35.33[a]	0.94 ± 0.03[a]

[a] $p < 0.01$ as compared with wild type.

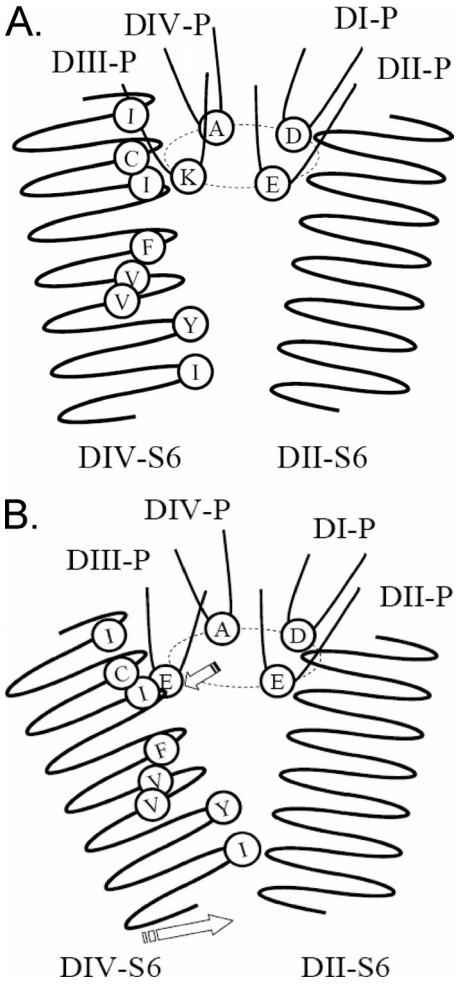

FIGURE 4. **Schematic representation of the proposed molecular mechanism underlying the I_{US} state.** Shown are the P-loops and the S6 segments of DII and DIV. *A*, the non-inactivated state is shown. Lys-1237 of DIII P-loop is located close to Ile-1575 of the DIV-S6 segment. *B*, mutation K1237E results in electrostatic repulsion between Glu-1237 and other negatively charged amino acids in the selectivity filter (Asp-400, Glu-755). This electrostatic repulsion gives rise to a swinging out of the DIII P-loop, resulting in an interaction between the Glu-1237 and the side chain of Ile-1575 (*upper arrow*). This interaction favors a conformational change of the DIV-S6 segment which gives rise to the I_{US} state (*lower arrow*).

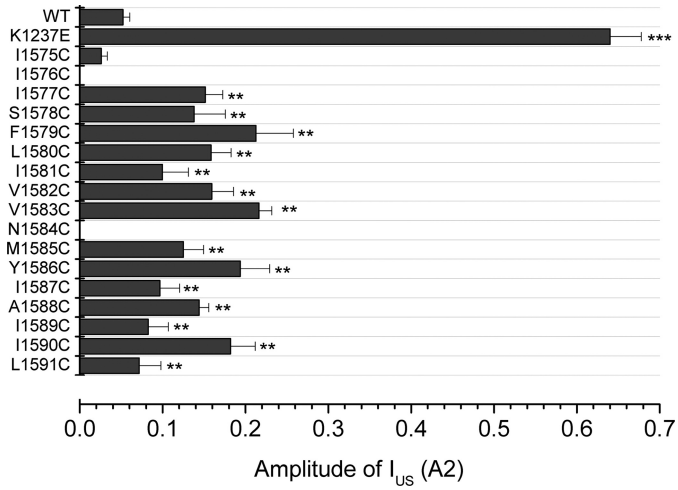

FIGURE 5. **Effect of cysteine scanning mutagenesis of the DIV-S6 segment on I_{US}.** Shown is the result of double exponential fits (Equation 1) to the time course of recovery from a prolonged depolarization as shown in Fig. 1*A*. Because of the low amplitude of recovery from I_{US} in these mutants, the parameter τ_2 was fixed at 120 s during the fitting procedure. The *asterisks* indicate significant differences from wild type (**, $p < 0.01$; ***, $p < 0.001$; $n = 5$–7). With the exception of I1575C, all mutants significantly enhanced recovery from I_{US}, indicating a role of the DIV-S6 segment in the generation of the I_{US} state. Mutants I1576C and N1584C did not express sufficient current to be studied.

mutations in the selectivity filter would alter the function of the I_{US} gate in DIV-S6, and mutations in DIV-S6 might alter the functional properties of the selectivity filter. To address this issue we explored the effect of selected mutations in the DIV-S6 segment on the selectivity of permeation in K1237E. To this end we studied the change in the reversal potential produced by replacing Na^+ (90 mM) as the major permeating cation by choline (90 mM). The observed shifts in reversal potential were used to calculate the respective changes in relative permeabilities (see "Experimental Procedures"). We found that both K1237E/I1575A and K1237E/I1575C significantly improved the selectivity of permeation for Na^+, whereas the mutation K1237E/F1579A, which did not reduce entry into I_{US}, also had no effect on the selectivity of permeation (Fig. 9). These data argue for a mutual interaction between gating and selectivity of the sites DIV-1575 and DIII-1237.

Molecular Rearrangements in the Selectivity Filter Probed by Energy Minimization in a Published Homology Model of the Voltage-gated Na^+ Channel—We have used a previously published homology model of the voltage-gated Na^+ channel to investigate possible molecular rearrangements within the selectivity filter, produced by mutations at sites 1237 of the P loop of DIII and site 1575 of DIV-S6 (K1237E and K1237E/I1575A) (2). The selectivity filter of the Na^+ channel is

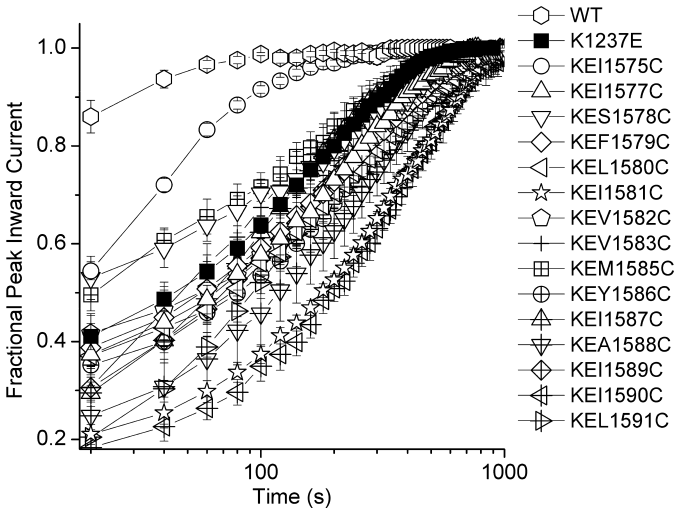

FIGURE 6. **Effect of addition of serial DIV-S6 cysteine mutations on I_{US} produced by K1237E.** Experiments were performed as in Fig. 1. Shown is the normalized time course of recovery from inactivation as in Fig. 3. To allow better discrimination between the graphs, a log scale was chosen for the time axis. The time course of recovery in K1237E/I1575C was significantly faster than in all other double mutants. $n = 3–7$.

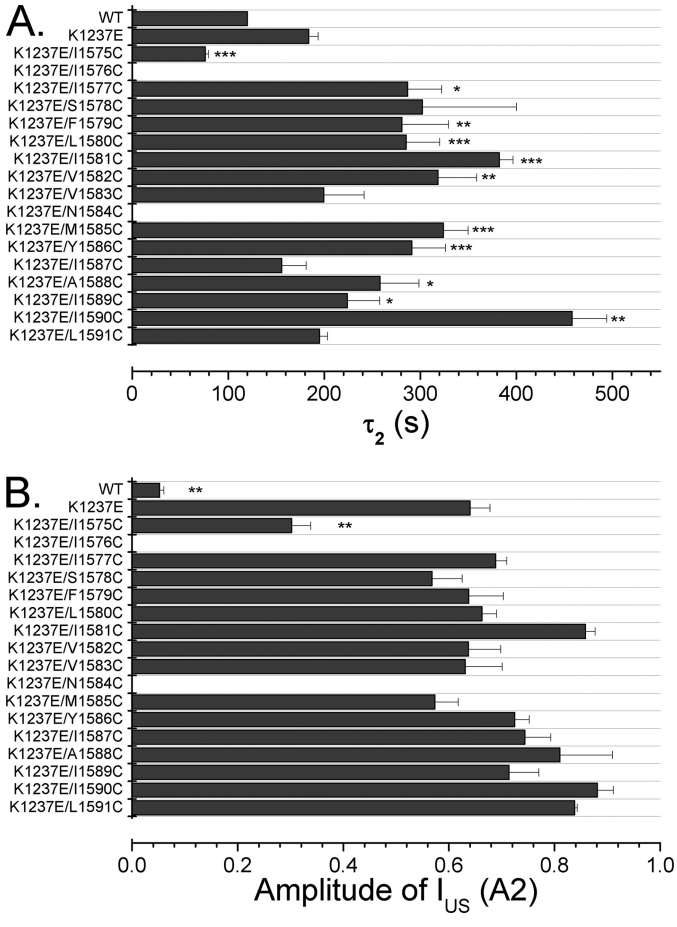

FIGURE 7. **Modulating effect of serial cysteine mutagenesis of the DIV-S6 segment on I_{US} produced by the mutation K1237E.** Shown are the results of fitting Equation 1 to the data points in Fig. 6. *Asterisks* denote significant difference from K1237E (*, $p < 0.05$; **, $p < 0.01$; ***, $p < 0.001$, $n = 3–7$). Most S6 mutations increased both the time constant of recovery from I_{US} and the fraction of channels recovering from I_{US}. Only in K1237E/I1575C both time constants and amplitude were reduced.

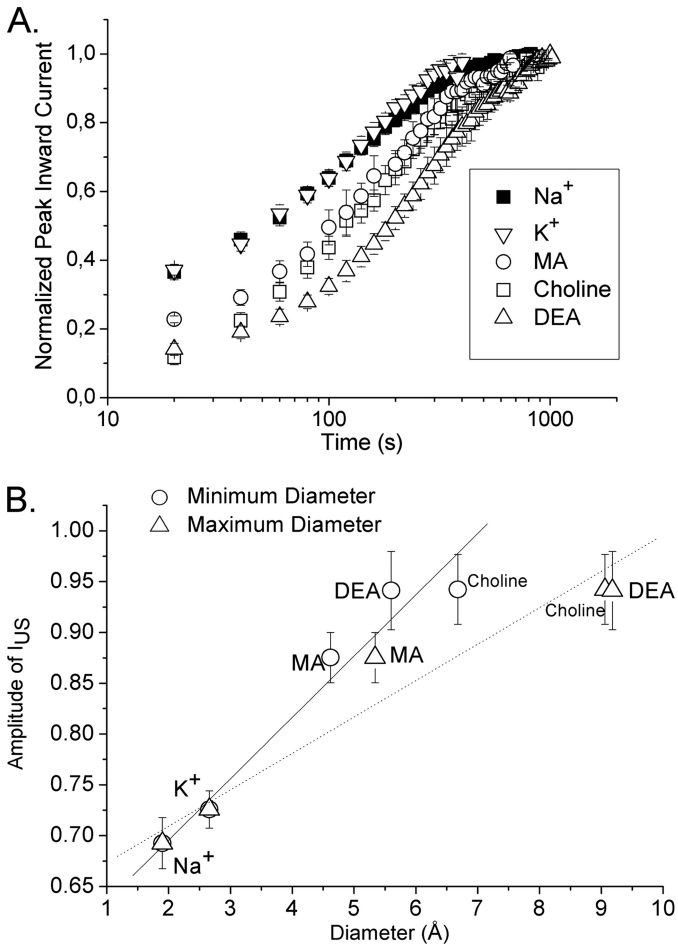

FIGURE 8. **Passage of large organic cations through the pore increases the likelihood of entry into I_{US}. Presumably, the passage of large organic cations through the selectivity filter is associated with an increase in diameter of the pore.** If I_{US} results from a widening of the pore, then the permeation of large cations should increase the likelihood of entry into I_{US}. *A*, recovery from the I_{US} state was assessed in K1237E. The voltage clamp protocol and data analysis were the same as shown in Figs. 1 and 3. The following charge carriers were assessed (90 mM, $n = 3–6$): Na^+, K^+, choline, methylammonium (*MA*), and diethylammonium (*DEA*). When Na^+ was the permeating ion, I_{US} recovered with a time constant of 155 ± 12 s. This time constant increased during permeation with K^+ (175 ± 19 s), MA (208 ± 25 s), choline (208 ± 58 s), and DEA (351 ± 51 s). The amplitudes of I_{US} were only slightly increased during permeation with K^+. Permeation with large organic cations resulted in a substantial increase in the amplitude of I_{US} ($p < 0.05$, see *panel B* for data). *B*, correlation between the size of permeating ions and the increase in amplitude of I_{US} is shown. As the parameter of molecular size, we used the diameter calculated from the Pauling ionic radii for Na^+ and K^+. For the organic cations we calculated the minimum and maximum diameter by using the functions *Minimum projection* radius and *maximum projection* radius of the software marvinSketch. Both minimum and maximum diameter were significantly correlated with the amplitude of I_{US} ($p < 0.01$).

formed by the side chains of four residues (DEKA motif) and is normally blocked by a hydrogen bond to the side chain of lysine of DIII (26). As shown in Fig. 10*A* in the wild type channel, the side chain of Glu-755 (DII) interacts directly with Lys-1237 (DIII) via a hydrogen bond. The strong electrostatic interaction of the side chain of Lys-1237 with Glu-755 and also Asp-400 is an important stabilizing factor for the spatial structure of the outer vestibule of the Na^+ channel. The bulky nonpolar side chain of Ile-1575 also stabilizes the structure by making optimal steric (van der Waals) contacts and hydro-

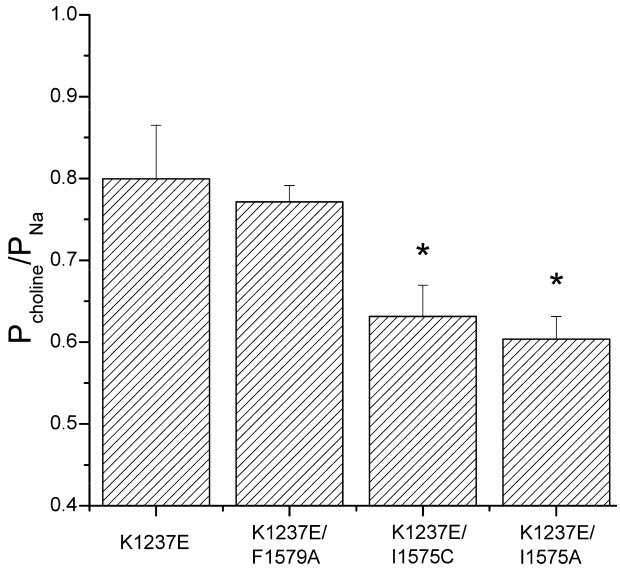

FIGURE 9. **Mutations I1575A and I1575C increase selectivity for Na$^+$ ions in K1237E.** The permeability of the channels for the large organic cation choline was assessed from the shift in reversal potential produced by replacing 90 mM Na$^+$ of the bath solution with 90 mM choline. Current-voltage relationships were fit with the function Equation 2 to derive the reversal potential. Permeability ratios were then calculated from the shift in reversal potential with Equation 3. In K1237E/I1575A and K1237E/I1575C permeability to choline was significantly smaller than in K1237E alone or in the double mutant K1237E/F1579A, indicating that the mutations at site 1575 reduce the diameter of the selectivity filter ($n = 6$ for each construct).

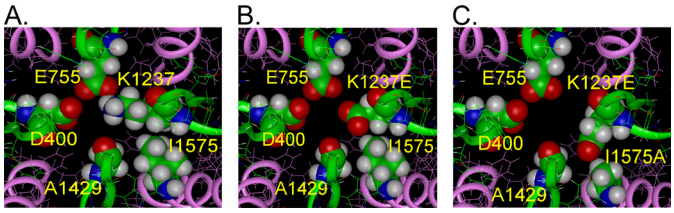

FIGURE 10. **Molecular model of the conformational changes inside the selectivity filter associated with I_{US}.** Shown are the amino acid residues at the internal turn of the P-loops (*green ribbons*) forming the selectivity filter: DIAsp-400, DII-Glu-755, DIII-Lys-1237, DIV-Ala-1529. The adjacent S6 segments are represented by *pink ribbons*. *A*, wild type rNa$_V$1.4 is shown. Lys-1237 is in close proximity to Glu-755 and Ile-1575 of DIV-S6. *B*, mutation K1237E gives rise to an electrostatic repulsion between Glu-755 and Glu-1237, resulting in a lateral displacement of Glu-1237, thereby establishing an interaction with Ile-1575. *C*, the additional mutation I1575A produces a further displacement of the side chain of Glu-1237 in the direction of Ala-1575. Glu-755 and Glu-1237 are now separated by a bulky water molecule (not shown) with a high dielectric constant that removes the strong electrostatic repulsion between these side chains.

phobic interactions with the alkyl part of the side chain of Lys-1237. The substitution of Lys-1237 by glutamic acid introduces a strong electrostatic destabilization of the selectivity filter and the structure of the outer vestibule due to the proximity of the carboxylate groups of Asp-400, Glu-755, and K1237E (Fig. 10*B*). The electrostatic repulsion between Glu-755 and Glu-1237, even in their optimal location in this mutant, is still substantial (+7 kcal/mol). This repulsion would result in a lateral movement of Glu-1237; however, the conformational change of its side chain is prevented by the bulky side chain of Ile-1575 in the proximity of Glu-1237. Hence, the position of the side chain of the residue at site 1237 is practically the same as in Fig. 10*A*. This electrostatic destabilization of the system in the case of the K1237E mutation could produce structural changes, leading to I_{US}.

As shown in Fig. 4*B*, we suggest that in the mutant K1237E the DIV-S6 segment changes its conformation or position, which ultimately leads to a collapse of the internal vestibule. It should be noted that the DIV-S6 segment does not contain a flexible "glycine hinge" such that conformational changes at the level of the selectivity filter may easily be transmitted to more internal parts of the helix. However, the additional substitution of Ile-1575 by alanine creates an open space around site 1575 that allows for a reorientation of Glu-1237 toward Ala-1575 (Fig. 10*C*). As a consequence, the side chains of Glu-755 and Glu-1237 are now separated by bulky water molecules with a high dielectric constant, which also reduces the electrostatic repulsion between these side chains (not shown). This may lead to a weakening of the interaction between Glu-1237 and Ala-1575, thereby allowing for a reorientation of the DIV-S6 segment, which reduces the probability of entry into I_{US}. The simulation demonstrates that the mutation I1575A in the background of K1237E creates a new electrostatic environment in the selectivity filter that may account for the observed changes in selectivity. A direct interaction between amino acids at sites 1237 and 1575 is also suggested by the fact that the magnitude of the effect on I_{US} in K1237E by additional mutations at site 1575 appeared to be related to the length and/or volume of the side chain of the replaced amino acid. Thus, the replacement of Ile-1575 by cysteine resulted in a smaller reduction of the amplitude of ultra-slow recovery than replacement by alanine (Table 1, Fig. 7*B*). The van der Waals volume of cysteine 86 Å^3 is intermediate between the native isoleucine (124 Å^3) and alanine (67 Å^3; Ref. 27).

Ile-1575 Is Highly Conserved in Na$^+$ Channels—Our data suggest that Ile-1575 controls the interaction between DIV-S6 and the selectivity filter and may, therefore, serve a significant purpose in ion channel function. Thus, it appears of interest to explore the degree of conservation of this residue across different species. To this end we retrieved 131 Na$^+$ channel sequences from the UniProt data base and aligned the sequences of the DIV-S6 segments. The supplemental Table 1 shows that isoleucines are conserved at positions homologous to 1575 in rNa$_V$1.4 in all vertebrate sequences (Na$^+$ channel sequences 1–89). Only a number of insect Na$^+$ channels carry a homologous substitution by leucine at this site (Na$^+$ channel sequences 90–127). In three non-vertebrate channels we found substitutions by valine (Na$^+$ channel sequences 128–130) and in one channel by methionine (Na$^+$ channel sequence 131).

DISCUSSION

Early in site-directed mutagenesis studies of ion channels, it became clear that the selectivity filter is a part of the gating machinery. The involvement of the outer vestibule in channel gating has been extensively investigated in K$^+$ channels, which upon depolarization can enter into a slow inactivated state called "C-type inactivation" (28). Early functional studies strongly suggested that C-type inactivation involves a three-dimensional rearrangement of the outer channel vestibule (29–33). More recently, these functional data have been con-

firmed by structural studies in the bacterial KcsA channel (8, 34, 35).

Involvement of the Inner Vestibule in C-type Inactivation—In addition to the ample evidence for a conformational change of the outer vestibule as the molecular mechanism in C-type inactivation, recent studies suggest that the inner vestibule may also be involved in C-type inactivation. Thus, in $K_V1.4$ channels slow inactivation is associated with a decrease in intracellular aqueous pore volume (36), pointing toward a significant role of the inner vestibule in slow inactivation gating. A number of other recent studies suggest that slow inactivation in K^+ channels is associated with conformational changes both of the outer mouth and the internal cavity (9, 36–39).

Slow Inactivation in Voltage-gated Na^+ Channels—In voltage-gated Na^+ channels the time constants of entry into and recovery from fast inactivation are on the order of milliseconds. The term "slow inactivation" refers to kinetic states whose lifetimes are one to several orders of magnitude greater than those of the fast inactivated state. Na^+ channels are believed to have several slow inactivated states that can be classified according to their time-course of recovery from inactivation (18). We have shown previously that certain mutations in the selectivity filter region promote an ultra-slow inactivated state; entry into and exit from I_{US} requires up to 20 min (10, 11, 40). In terms of the structural underpinnings of slow inactivation in Na^+ channels, it has been suggested that these forms of inactivation occur by a closure of the extracellular mouth of the channel (10, 11, 18, 23, 40–46). However, this idea has recently been challenged by the demonstration that accessibility of cysteines, engineered to some positions in the outer vestibule, to a charged sulfhydryl modifying agent was preserved during slow inactivation (47).

There is substantial experimental evidence suggesting that the internal vestibule of Na^+ channels is involved in slow inactivation gating; a number of mutations in S6 segments have been reported to affect slow inactivated states (48–55). Furthermore, accessibility of an engineered cysteine in the middle of the DIV-S6 helix for 2-aminoethylmethane thiosulfonate applied from the cytoplasmic side depends on the duration of the preceding depolarization, revealing two conformational changes near this site; that is, one coupled to fast inactivation and one tightly associated with slow inactivation (53).

Another argument for the involvement of the inner vestibule in slow inactivation relates to the fact that Na^+ channels are major targets of G protein-coupled receptor signaling cascades that lead to the activation of serine/threonine protein kinases (56). G protein-coupled receptor- and protein kinase-dependent reductions in Na^+ channel availability have recently been shown to be mediated by modulation of slow inactivation (57). The location of the PKA/PKC phosphorylation site is in the intracellular linker between DI and DII. Hence slow inactivation must be associated with a conformational change of the intracellular parts of the channel.

In summary, both the outer and the inner vestibule may be involved in the generation of slow inactivated states. This raises the question of whether there is a molecular "switch" between the outer and the inner vestibule responsible for the transmission of conformational changes between these regions.

Experimental Evidence Suggesting a Cross-talk between Internal and External Vestibule in Voltage-gated Na^+ Channels—Ong *et al.* (44) reported that the rate of sulfhydryl modification of a cysteine engineered to the outer vestibule was drastically reduced when the Na^+ channel blocker lidocaine was bound to the internal vestibule. Obviously, when bound to the internal vestibule, lidocaine induced a conformational rearrangement of the external vestibule, indicating a kinetic connection between these sites (44). Later, the same group demonstrated that the drug-specific kinetics of binding to slow inactivated states by lidocaine and bupivacaine closely matched the kinetics of sulfhydryl modification of a cysteine engineered to the outer vestibule (58). Yamagishi *et al.* (59) observed that application of external QX314 (a membrane-impermeant quaternary derivative of lidocaine) did not block $rNa_V1.4$ channels but nevertheless slowed recovery from internal block by QX314, suggesting an allosteric effect of external QX314 binding on recovery from internal block. In the $rNa_V1.2$ channel a potential interaction between Trp-1716 in the DIV-P-loop (corresponding to Trp-1531 in $rNa_V1.4$) and Phe-1764 in the DIV-S6 segment (corresponding to Phe-1579 in $rNa_V1.4$) was recently reported, being closely related to anticonvulsant and/or local anesthetic binding (60). In summary, these data are highly suggestive of an intramolecular communication between the outer and the internal vestibule of voltage-gated Na^+ channels.

The Present Study—The present study was designed to explore possible links between the outer and the internal vestibule of the $rNa_V1.4$ channel. To this end we studied the modulation of the previously characterized ultra-slow inactivated state by a mutation in the outer vestibule, mutations in the inner vestibules, and combinations of both. The involvement of the outer and the inner vestibule in this state was suggested by the finding that molecules interacting with the outer and with the internal vestibule affected I_{US} (10, 12, 14, 40).

After 5 min of depolarization, $<$20% of wild type channels recover from I_{US} (Fig. 1*B*). However, a mutation in the selectivity filter, K1237E, substantially promotes entry into the I_{US} state (Fig. 1*B*). Enhanced entry into I_{US} is also produced by the mutations F1579A and Y1586A in the DIV-S6 segment (Fig. 3, Table 1). These amino acids are considered to face the pore internal to the selectivity filter (Fig. 1*B*). Amino acid Ile-1575 of DIV-S6 is also considered to face the pore but in close proximity to Lys-1237 of the domain III P-loop. In contrast to F1579A and Y1586A, I1575A did not favor entry into I_{US} (Fig. 3*A*, Table 1). The addition of the DIV-S6 mutations F1579A or Y1586A to K1237E resulted in an even greater propensity to enter the I_{US} state than with K1237E alone (Fig. 3*B*). Conversely, mutation I1575A in the background of K1237E inhibited entry into I_{US} (Fig. 3*A*). In fact, the fraction of channels recovering from I_{US} in double mutant K1237E/I1575A was not different from wild type. This suggests that site 1575 may have a special role in the generation of the I_{US} state.

Next, we produced serial replacements of DIV-S6 amino acids by cysteine. The side chain of cysteine is both larger and more reactive than that of alanine. Presumably, replacement of the native amino acids by cysteine will impose greater structural changes in DIV-S6 than mutations to alanine. Most of the single cysteine replacements produced a mild enhancement of the I_{US} state. Only I1575C retained wild type character (Fig. 5). Thus, neither I1575A nor I1575C affected the propensity to enter the I_{US} state. As to the double mutants, all constructs either did not change the amount of I_{US} in K1237E or enhanced I_{US}, with the exception of I1575C (Figs. 6 and 7). Although K1237E/I1575C did not reduce the I_{US} state to the same degree as K1237E/I1575A, the mutant substantially reduced the time constant of recovery from I_{US} (Fig. 7*A*) and decreased the stability of this state (Fig. 4). The different amount of reduction of the I_{US} state produced by K1237E/I1575A and K1237E/1575C may be due to the higher reactivity and larger size of cysteine compared with alanine. These results support the idea that site 1575 has a unique role in the generation of the I_{US} state.

Because K1237E channels are permeable for large cations, this mutation is considered to produce a widening of the selectivity filter. This widening may be due to a lateral "swinging out" of the DIII-P loop, perhaps caused by an electrostatic repulsion between residue Glu-1237 and residues Asp-400 and/or Glu-755 (Fig. 4*B*). Such swinging out has been suggested by Huang and Moczydlowski (21) to explain the permeation of $rNa_V1.4$ channels by spermidine at high voltages. The lateral movement of the DIII-P loop may give rise to an interaction between the DIV-S6 and Ile-1575. The resulting conformational change in DIV-S6 then generates the I_{US} state, perhaps by a constriction of the internal vestibule (Fig. 4). The latter idea is supported by the fact that the presence of lidocaine in the internal vestibule prevents entry into the I_{US} state by a foot-in-the-door mechanism (14). The concept of a widening of the selectivity filter as a primary mechanism in the generation of I_{US} is supported by the fact that permeation of the channel with large cations increases the fraction of channels recovering from the I_{US} state in a size-dependent fashion (Fig. 8). Alternatively, the increase in the fraction of K1237E channels recovering from I_{US} by permeation with large cations may have resulted from depletion of Na^+ ions from the pore. Indeed, lowering the concentration of permeating Na^+ ions has been shown to increase slow inactivation (41, 62). However, by contrast to slow inactivation, *ultra-slow inactivation* is not sensitive to lowering of external $[Na^+]$ (12).

The interaction between the DIV-S6 segment and the selectivity filter appears to be mutual. As mentioned above, amino acids I1575A, F1579A and Y1586A are predicted to face the pore in close proximity to the selectivity filter. We investigated whether the size of the selectivity filter, reflected by the permeability to choline is associated with the propensity to enter the I_{US} state. As shown in Fig. 9 those double mutants that are resistant to I_{US} are significantly less permeable to choline than those which readily enter I_{US}. Thus, the conformational change that gives rise to the I_{US} state also interferes with the function of the selectivity filter. It should be mentioned that the conclusion of these experiments is limited by the fact that using the two electrode voltage clamp technique a control over the ionic composition of the interior of the oocytes is not possible. We have to assume that the ionic composition of the oocytes remains stable throughout the experiment. However, the two-electrode voltage clamp technique in *Xenopus laevis* oocytes has been applied previously to derive permeability ratios for mutations in the outer vestibule of the $rNa_V1.4$ channel (17).

The mutant K1237R has been found to reduce the Na^+/K^+ selectivity by approximately the same degree as K1237A (19). However, in contrast to K1237A, K1237R does not promote entry into the I_{US} state. This may argue against our theory of a lateral swinging out of Glu-1237-generating I_{US} (Fig. 4*B*), because according to the mentioned change in selectivity, such a swing out should also be present in K1237R. On the other hand, K1237A but not K1237R, is permeable to Ca^{2+} ions (19). Furthermore, the permeability to the large cation methylammonium is intermediate between K1237A (not resistant to I_{US} ; Ref. 15) and wild type (resistant to I_{US} ; Ref. 63). Thus, the size of the selectivity filter in K1237R is probably smaller than in K1237E, and the same may hold true for the distance of the lateral movement of the DIII P-loop. These data also indicate that the amount of lateral movement necessary to give rise to a contact with the S6 segment is probably very small.

Previous Reports Suggesting a Pivotal Role of Residue Ile-1575 with Regard to the Structure of the Channel—In $rNa_V1.2$ channels the analogous mutation I1760A creates an access pathway between the local anesthetic receptor and the extracellular medium for the membrane impermeant local anesthetic QX-314 (64). Similar findings have been obtained in other Na^+ channel isoforms including $Na_V1.4$ (20, 65–68). The access route for QX-314 was not through the outer vestibule because the R13N mutant of μ-conotoxin GIIIA, which partially occludes the channel pore from the outside, did not inhibit access by QX-314 (20). In a recently published homology model of the voltage-gated Na^+ channel, Ile-1575 is part of a "tunnel" formed by the inner helices of DIII and DIV and the pore helix of DIII forming an extracellular access route by which local anesthetic drugs can reach their binding site in the inner cavity (69, 70). These data underscore the importance of a close spatial relationship between Ile-1575 and the selectivity filter.

Comparison with Structural Data from K^+ Channels—Crystal structures of voltage-gated Na^+ channels are currently unavailable. On the other hand, a number of published K^+ channel crystal structures may allow further insights into the mechanical underpinnings of ion channel gating. As mentioned earlier, Cuello *et al.* (8, 9) recently solved the structure of KcsA in its fully open conformation and in a number of partial openings, representing "snapshots" of the channel activation-inactivation pathway. These structures suggested that in the open state of KcsA residue Phe-103 in TM2 interacts with the C-terminal end of the pore α-helix, compressing the pitch of its first helical turn. As a consequence, the structure of the selectivity filter is altered, leading to a non-conductive conformation. Perturbation mutagenesis at position 103 af-

fected gating kinetics, as predicted from their structural analysis; small side-chain substitutions F103A and F103C severely impaired inactivation kinetics, suggesting an allosteric coupling between the inner helical bundle and the selectivity filter. Molecular dynamics suggested significant non-polar van der Waals interaction between Phe-103 and Thr-74/75 at the C-terminal end of the pore helix of the same subunit and Ile-100 located in the middle of TM2 of the neighboring subunit. Interaction-energy calculations suggested that in the mammalian voltage-gated $K_V1.2$ channel Ile-402 (homologous to Phe-103 in KcsA) has a strong van der Waals coupling with Thr-372 and Thr-373 (homologous to Thr-73 and Thr-74 in KcsA). In the Shaker K_V channel Ile-470 is homologous to Phe-103 in KcsA. Mutations of Ile-470 in Shaker to alanine (9) or cysteine (71, 72) destabilize the C-type inactivated state. In summary, C-type inactivation in K^+ channels occurs by an interaction of amino acids in the pore-lining of the inner vestibule with amino acids located close to the selectivity filter in the outer vestibule.

There are several similarities between the mechanism of I_{US} proposed in this study for Na_V channels and the mechanism of C-type inactivation as suggested by the published KcsA crystal structures. First, in both cases a residue in the middle of the pore-forming transmembrane segment (S6 in Na_V and K_V channels, TM2 in KcsA) interacts with an amino acid at the cytoplasmic turn of the P-loop. Second, both C-type inactivation and I_{US} are destabilized by replacement of amino acids with short side chains. Third, both in Na_V and K_V channels the proposed interacting residue in the S6 segment is a highly conserved isoleucine (see the supplemental Table 1 and Fig. S10 in Ref. 9).

On the other hand, although Cuello *et al.* (9, 39) propose C-type inactivation to occur by an interaction between the outer and the inner vestibule of the same subunit, our data suggest an interaction between the P-loop and the S6 segment of different, adjacent domains. To interpret the findings of this study in the context of published crystal structures, we first consider an alignment between the inner helices of KcsA, Shaker, $K_V1.2$, and the DIV-S6 helix of $rNa_V1.4$ (Fig. 11). The K^+ channel sequences are aligned with respect to the highly conserved "gating hinge" glycine. The DIV-S6 helix of $rNa_V1.4$ does not contain a glycine, but Ser-1578 aligns with glycines in the middle of the S6 helices of domains II and III and is, therefore, most probably homologous to Gly-99 in KcsA (2). Clearly, the residues Phe-103 and Ile-470, which control inactivation in KcsA and Shaker, are homologous to Ile-402 in $K_V1.2$ (8, 9). However, Ile-1575 of $rNa_V1.4$ is located 7 amino acids N-terminal to the position equivalent to Phe-103 in KcsA. Thus, in terms of the amino acid sequence, Phe-103 seems not to be equivalent to Ile-1575. On the other hand, as shown in Fig. 12, the amino acids equivalent to Ile-1575 in KcsA (Met-96) and in $K_V1.2$ (Ala-395) are in close proximity to Thr-74 (KcsA) and Thr-373 ($K_V1.2$) at the inner tip of the selectivity filter of the neighboring subunit. This molecular relationship closely resembles the arrangement of Ile-1575 and Lys-1237 in the Lipkind-Fozzard model. Functional data support a role of the position equivalent to Met-96 in KcsA with regard to inactivation gating; mutations at the

KcsA	Shaker	$K_V1.2$	$Na_V1.4$
W 87	W 454	G 386	I 1566
G 88	G 455	G 387	G 1567
R 89	K 456	K 388	I 1568
L 90	I 457	I 389	C 1569
V 91	V 458	V 390	F 1570
A 92	G 459	G 391	F 1571
V 93	S 460	S 392	C 1572
V 94	L 461	L 393	S 1573
V 95	C 462	C 394	Y 1574
M 96	A 463	A 395	**I 1575**
V 97	I 464	I 396	I 1576
A 98	A 465	A 397	I 1577
G 99	***G 466***	***G 398***	***S 1578***
I 100	V 467	V 399	F 1579
T 101	L 468	L 400	L 1580
S 102	T 469	T 401	I 1581
F 103	**I 470**	**I 402**	V 1582
G 104	A 471	A 403	V 1583
L 105	L 472	L 404	N 1584
V 106	P 473	P 405	M 1585
T 107	V 474	V 406	Y 1586
A 108	P 475	P 407	I 1587
A 109	V 476	V 408	A 1588
L 110	I 477	I 409	I 1589
A 111	V 478	V 410	I 1590
T 112	S 479	S 411	L 1591

FIGURE 11. **Ile-402 in $K_V1.2$ channel is homologous to Ile-470 in Shaker.** Amino acid sequence alignment of inner helices between KcsA, Shaker, $K_V1.2$, and DIV-S6 of $rNa_V1.4$ is shown. *Underlines*, residues homologous to Ile-1575 in $rNa_V1.4$. *Box*, glycine hinge residues. *Light Gray*, residues homologous to Phe-103 in the KcsA channel.

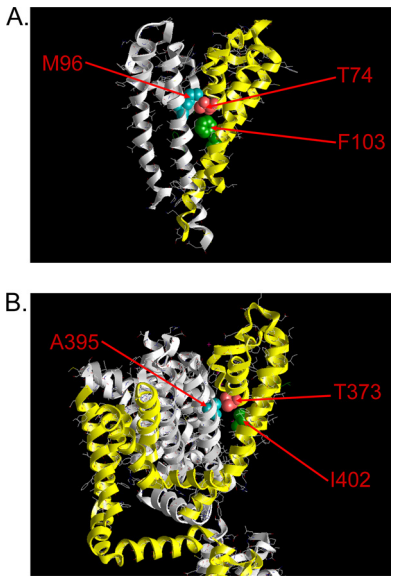

FIGURE 12. **Close spatial relationship between gating-sensitive amino acids in the outer and the inner vestibule of K^+ channel crystal structures.** Shown are two of the four subunits of the published structures of KcsA (bacterial, non-voltage gated; Protein Data Bank code 1BL8 (1)) and mammalian, voltage gated ($K_V1.2$, Protein Data Bank Protein Data Bank code 2A79 (61)). For clarity, protein backbone ribbons are colored differently for each subunit. Key amino acid side chains are shown as van der Waals spheres (*blue*, amino acid at position equivalent to site 1575 in $rNa_V1.4$; *rose*, amino acid at the inner turn of the P-loop, possible equivalent to Lys-1237 in $rNa_V1.4$; *green*, amino acid for which a major interaction with the P-loop is proposed to account for C-type inactivation in KcsA (9). *A*, KcsA; Thr-74 of one subunit (P-loop; *yellow ribbon*) is in close relationship to Met-96 (TM2) of the adjacent subunit (*white ribbon*) and with Phe-103 (TM2) of the same subunit. *B*, $K_V1.2$; Thr-373 of one subunit (*yellow ribbon*) is close to Ala-395 of the adjacent subunit (*white ribbon*) and to Ile-402 of the same subunit.

analogous site in Shaker (Ala-463) have been shown to modulate C-type inactivation (73, 74). The same holds true for the Shaker analog (Thr-441) of the potential interaction partner Thr-74 (KcsA), Thr-373 (K_V1.2) in the outer vestibule (Fig. 12; Ref. 75). This structural analysis in combination with the presented functional data suggests that interactions between the inner and the outer vestibule may represent a common gating mechanism in ion channels.

Acknowledgments—We thank Dr. John W. Kyle (Cardiac Electrophysiology Laboratories, The University of Chicago) for helpful advice with engineering of the constructs. The pictures in Fig. 12 were generated by the MVM graphics program, by ZMM Software Inc. (Dr. Boris S. Zhorov, Dept. of Biochemistry and Biomedical Sciences, McMaster University, Hamilton, Ontario, Canada).

REFERENCES

1. Doyle, D. A., Morais, Cabral, J., Pfuetzner, R. A., Kuo, A., Gulbis, J. M., Cohen, S. L., Chait, B. T., and MacKinnon, R. (1998) *Science* **280,** 69–77
2. Lipkind, G. M., and Fozzard, H. A. (2000) *Biochemistry* **39,** 8161–8170
3. Yifrach, O., and MacKinnon, R. (2002) *Cell* **111,** 231–239
4. Sadovsky, E., and Yifrach, O. (2007) *Proc. Natl. Acad. Sci. U.S.A.* **104,** 19813–19818
5. Shang, L., and Tucker, S. J. (2008) *Eur. Biophys. J.* **37,** 165–171
6. Rosenhouse-Dantsker, A., and Logothetis, D. E. (2006) *Biophys. J.* **91,** 2860–2873
7. Panyi, G., and Deutsch, C. (2006) *J. Gen. Physiol.* **128,** 547–559
8. Cuello, L. G., Jogini, V., Cortes, D. M., and Perozo, E. (2010) *Nature* **466,** 203–208
9. Cuello, L. G., Jogini, V., Cortes, D. M., Pan, A. C., Gagnon, D. G., Dalmas, O., Cordero-Morales, J. F., Chakrapani, S., Roux, B., and Perozo, E. (2010) *Nature* **466,** 272–275
10. Todt, H., Dudley, S. C., Jr., Kyle, J. W., French, R. J., and Fozzard, H. A. (1999) *Biophys. J.* **76,** 1335–1345
11. Hilber, K., Sandtner, W., Kudlacek, O., Schreiner, B., Glaaser, I., Schütz, W., Fozzard, H. A., Dudley, S. C., and Todt, H. (2002) *J. Biol. Chem.* **277,** 37105–37115
12. Szendroedi, J., Sandtner, W., Zarrabi, T., Zebedin, E., Hilber, K., Dudley, S. C., Jr., Fozzard, H. A., and Todt, H. (2007) *Biophys. J.* **93,** 4209–4224
13. Ragsdale, D. S., McPhee, J. C., Scheuer, T., and Catterall, W. A. (1996) *Proc. Natl. Acad. Sci. U.S.A.* **93,** 9270–9275
14. Sandtner, W., Szendroedi, J., Zarrabi, T., Zebedin, E., Hilber, K., Glaaser, I., Fozzard, H. A., Dudley, S. C., and Todt, H. (2004) *Mol. Pharmacol.* **66,** 648–657
15. Hilber, K., Sandtner, W., Zarrabi, T., Zebedin, E., Kudlacek, O., Fozzard, H. A., and Todt, H. (2005) *Biochemistry* **44,** 13874–13882
16. Lipkind, G. M., and Fozzard, H. A. (1994) *Biophys. J.* **66,** 1–13
17. Tsushima, R. G., Li, R. A., and Backx, P. H. (1997) *J. Gen. Physiol.* **109,** 463–475
18. Kambouris, N. G., Hastings, L. A., Stepanovic, S., Marban, E., Tomaselli, G. F., and Balser, J. R. (1998) *J. Physiol.* **512,** 693–705
19. Favre, I., Moczydlowski, E., and Schild, L. (1996) *Biophys. J.* **71,** 3110–3125
20. Sunami, A., Glaaser, I. W., and Fozzard, H. A. (2001) *Mol. Pharmacol.* **59,** 684–691
21. Huang, C. J., and Moczydlowski, E. (2001) *Biophys. J.* **80,** 1262–1279
22. Tsushima, R. G., Li, R. A., and Backx, P. H. (1997) *J. Gen. Physiol.* **110,** 59–72
23. Xiong, W., Li, R. A., Tian, Y., and Tomaselli, G. F. (2003) *J. Gen. Physiol.* **122,** 323–332
24. Eriksson, M. A., and Roux, B. (2002) *Biophys. J.* **83,** 2595–2609
25. Sun, Y. M., Favre, I., Schild, L., and Moczydlowski, E. (1997) *J. Gen. Physiol.* **110,** 693–715
26. Lipkind, G. M., and Fozzard, H. A. (2008) *J. Gen. Physiol.* **131,** 523–529
27. Creighton, T. E. (1993) *Proteins: Structures and Molecular Properties*, 2 Ed., p. 141, W. H. Freeman and Co., New York
28. Hoshi, T., Zagotta, W. N., and Aldrich, R. W. (1991) *Neuron* **7,** 547–556
29. Choi, K. L., Aldrich, R. W., and Yellen, G. (1991) *Proc. Natl. Acad. Sci. U.S.A.* **88,** 5092–5095
30. López-Barneo, J., Hoshi, T., Heinemann, S. H., and Aldrich, R. W. (1993) *Receptors Channels* **1,** 61–71
31. Baukrowitz, T., and Yellen, G. (1995) *Neuron* **15,** 951–960
32. Yellen, G., Sodickson, D., Chen, T. Y., and Jurman, M. E. (1994) *Biophys. J.* **66,** 1068–1075
33. Liu, Y., Jurman, M. E., and Yellen, G. (1996) *Neuron* **16,** 859–867
34. Zhou, Y., Morais-Cabral, J. H., Kaufman, A., and MacKinnon, R. (2001) *Nature* **414,** 43–48
35. Cordero-Morales, J. F., Jogini, V., Lewis, A., Vásquez, V., Cortes, D. M., Roux, B., and Perozo, E. (2007) *Nat. Struct. Mol. Biol.* **14,** 1062–1069
36. Jiang, X., Bett, G. C., Li, X., Bondarenko, V. E., and Rasmusson, R. L. (2003) *J. Physiol.* **549,** 683–695
37. Panyi, G., and Deutsch, C. (2007) *J. Gen. Physiol.* **129,** 403–418
38. Bett, G. C., and Rasmusson, R. L. (2004) *J. Physiol.* **556,** 109–120
39. Cuello, L. G., Jogini, V., Cortes, D. M., Pan, A. C., Gagnon, D. G., Cordero-Morales, J. F., Chakrapani, S., Roux, B., and Perozo, E. (2009) *Biophys. J.* **96,** 381a (Abst. 1959)
40. Hilber, K., Sandtner, W., Kudlacek, O., Glaaser, I. W., Weisz, E., Kyle, J. W., French, R. J., Fozzard, H. A., Dudley, S. C., and Todt, H. (2001) *J. Biol. Chem.* **276,** 27831–27839
41. Townsend, C., and Horn, R. (1997) *J. Gen. Physiol.* **110,** 23–33
42. Tomaselli, G. F., Chiamvimonvat, N., Nuss, H. B., Balser, J. R., Pérez-García, M. T., Xu, R. H., Orias, D. W., Backx, P. H., and Marban, E. (1995) *Biophys. J.* **68,** 1814–1827
43. Balser, J. R., Nuss, H. B., Chiamvimonvat, N., Pérez-García, M. T., Marban, E., and Tomaselli, G. F. (1996) *J. Physiol.* **494,** 431–442
44. Ong, B. H., Tomaselli, G. F., and Balser, J. R. (2000) *J. Gen. Physiol.* **116,** 653–662
45. Vilin, Y. Y., Fujimoto, E., and Ruben, P. C. (2001) *Biophys. J.* **80,** 2221–2230
46. Xiong, W., Farukhi, Y. Z., Tian, Y., Disilvestre, D., Li, R. A., and Tomaselli, G. F. (2006) *J. Physiol.* **576,** 739–754
47. Struyk, A. F., and Cannon, S. C. (2002) *J. Gen. Physiol.* **120,** 509–516
48. Wang, S. Y., and Wang, G. K. (1997) *Biophys. J.* **72,** 1633–1640
49. Takahashi, M. P., and Cannon, S. C. (1999) *Biophys. J.* **76,** 861–868
50. O'Reilly, J. P., Wang, S. Y., and Wang, G. K. (2000) *Biophys. J.* **78,** 773–784
51. O'Reilly, J. P., Wang, S. Y., and Wang, G. K. (2001) *Biophys. J.* **81,** 2100–2111
52. Wang, S. Y., Russell, C., and Wang, G. K. (2005) *Biophys. J.* **88,** 3991–3999
53. Vedantham, V., and Cannon, S. C. (2000) *Biophys. J.* **78,** 2943–2958
54. Chen, Y., Yu, F. H., Surmeier, D. J., Scheuer, T., and Catterall, W. A. (2006) *Neuron* **49,** 409–420
55. Chancey, J. H., Shockett, P. E., and O'Reilly, J. P. (2007) *Am. J. Physiol. Cell. Physiol.* **293,** C1895–C1905
56. Cantrell, A. R., and Catterall, W. A. (2001) *Nat. Rev. Neurosci.* **2,** 397–407
57. Carr, D. B., Day, M., Cantrell, A. R., Held, J., Scheuer, T., Catterall, W. A., and Surmeier, D. J. (2003) *Neuron* **39,** 793–806
58. Fukuda, K., Nakajima, T., Viswanathan, P. C., and Balser, J. R. (2005) *J. Physiol.* **564,** 21–31
59. Yamagishi, T., Xiong, W., Kondratiev, A., Vélez, P., Méndez-Fitzwilliam, A., Balser, J. R., Marbán, E., and Tomaselli, G. F. (2009) *Mol. Pharmacol.* **76,** 861–871
60. Yang, Y. C., Hsieh, J. Y., and Kuo, C. C. (2009) *J. Gen. Physiol.* **134,** 95–113
61. Long, S. B., Campbell, E. B., and Mackinnon, R. (2005) *Science* **309,** 897–903
62. Chen, Z., Ong, B. H., Kambouris, N. G., Marbán, E., Tomaselli, G. F., and Balser, J. R. (2000) *J. Physiol.* **524,** 37–49

63. Huang, C. J., Favre, I., and Moczydlowski, E. (2000) *J. Gen. Physiol.* **115,** 435–454
64. Ragsdale, D. S., McPhee, J. C., Scheuer, T., and Catterall, W. A. (1994) *Science* **265,** 1724–1728
65. Wang, G. K., Quan, C., and Wang, S. (1998) *Pflugers Arch.* **435,** 293–302
66. O'Leary, M. E., Digregorio, M., and Chahine, M. (2003) *Mol. Pharmacol.* **64,** 1575–1585
67. Lee, P. J., Sunami, A., and Fozzard, H. A. (2001) *Circ. Res.* **89,** 1014–1021
68. Ramos, E., and O'leary, M. E. (2004) *J. Physiol.* **560,** 37–49
69. Tikhonov, D. B., and Zhorov, B. S. (2005) *Biophys. J.* **88,** 184–197
70. Bruhova, I., Tikhonov, D. B., and Zhorov, B. S. (2008) *Mol. Pharmacol.* **74,** 1033–1045
71. Holmgren, M., Smith, P. L., and Yellen, G. (1997) *J. Gen. Physiol.* **109,** 527–535
72. Olcese, R., Sigg, D., Latorre, R., Bezanilla, F., and Stefani, E. (2001) *J. Gen. Physiol.* **117,** 149–163
73. Ogielska, E. M., and Aldrich, R. W. (1999) *J. Gen. Physiol.* **113,** 347–358
74. Meyer, R., and Heinemann, S. H. (1997) *Eur. Biophys. J.* **26,** 433–445
75. Yool, A. J., and Schwarz, T. L. (1995) *Biophys. J.* **68,** 448–458